

Compressive sensing adaptation for polynomial chaos expansions

Panagiotis Tsilifis^{a,*}, Xun Huan^b, Cosmin Safta^b, Khachik Sargsyan^b, Guilhem Lacaze^b,
Joseph C. Oefelein^b, Habib N. Najm^b, Roger G. Ghanem^a

^a*Sonny Astani Department of Civil Engineering, University of Southern California, Los Angeles, CA 90089, USA*

^b*Sandia National Laboratories, 7011 East Avenue, Livermore, CA 94550, USA*

Abstract

Basis adaptation in Homogeneous Chaos spaces rely on a suitable rotation of the underlying Gaussian germ. Several rotations have been proposed in the literature resulting in adaptations with different convergence properties. In this paper we present a new adaptation mechanism that builds on compressive sensing algorithms, resulting in a reduced polynomial chaos approximation with optimal sparsity. The developed adaptation algorithm consists of a two-step optimization procedure that computes the optimal coefficients and the input projection matrix of a low dimensional chaos expansion with respect to an optimally rotated basis. We demonstrate the attractive features of our algorithm through several numerical examples including the application on Large-Eddy Simulation (LES) calculations of turbulent combustion in a HIFiRE scramjet engine.

Keywords: Polynomial Chaos, basis adaptation, compressive sensing, ℓ_1 -minimization, dimensionality reduction

1. Introduction

While the use of computer codes to represent complex physical phenomena has always been an integral part of uncertainty quantification (UQ), efforts toward adopting more realistic models often face computational challenges that must be overcome before meaningful quantitative analysis becomes possible. The need for a statistical exploration of the solution space is arguably the most pressing of these challenges, requiring repetitive simulation of the numerical code. The associated computational burden quickly becomes prohibitive, especially in the context of complex physical systems where each of these simulations is, by itself, already testing the limits of computational resources. In many important instances, the map from input random parameters to output quantities is highly nonlinear, limiting the value of standard statistical sampling techniques. In such cases, L_2 -based formalisms, such as polynomial chaos (PC) expansions have shown promise [22, 30, 40, 32]. These methods, however, by explicitly tracking each input stochastic parameter, are subject to the curse of dimensionality which is manifested by a factorial growth with the number of parameters, of the numerical simulations required to systematically explore parameter space. Significant efforts have been expanded recently to leverage the mathematical structure provided by an L_2 resolution to alleviate that computational burden with rigorous and tractable error control [1, 2, 47]. While no single approach works universally, successful model reduction strategies have addressed these challenges with either the construction of a model surrogate that replaces the expensive initial model [22, 39], or the representation of the model output as a mapping from a reduced input space [41, 36, 1, 2, 47, 9].

*Corresponding author

Email addresses: tsilifis@usc.edu (Panagiotis Tsilifis), xhuan@sandia.gov (Xun Huan), csafta@sandia.gov (Cosmin Safta), ksargsy@sandia.gov (Khachik Sargsyan), guilhem.lacaze@gmail.com (Guilhem Lacaze), joseph.oefelein@aerospace.gatech.edu (Joseph C. Oefelein), hnnajm@sandia.gov (Habib N. Najm), ghanem@usc.edu (Roger G. Ghanem)

In this paper, we concentrate our efforts on approximating *nonlinear* response surfaces by polynomial chaos expansions that consist of *linear* series of terms that are orthogonal with respect to the probability measure of input variables. The foundation of these representations was pioneered in the context of stochastic finite elements [22, 19, 20, 21, 18, 53, 32], and the Hilbertian structure of the underlying L_2 space permitted the development of non-intrusive approaches for estimating the expansion coefficients [30, 3, 31]. More recently, basis enrichment [23], least-squares [4, 15] and ℓ_1 -minimization methods [6, 13, 16, 38] were suggested as enhancements or alternatives to the spectral perspective. Further, recent advances of ℓ_1 -minimization have demonstrated additional sparsity enhancement by adaptively selecting the basis terms [42, 28].

A recently introduced dimension reduction technique consists of a basis adaptation procedure [47] which constructs polynomial chaos expansions for specific quantities of interest (QoIs) using only a small number of Gaussian variables that are linear combinations of the original basis. These combinations are specifically adapted to the QoI in question and are obtained through a learning process which involves exploring the solution space through a limited number of samples. Standard basis adaptation procedures involve choosing these linear combinations through a rotation matrix computed according to particular sparse grid rules, following a low-dimensional quadrature rule for evaluating the adapted expansion for the QoI. While basis adaptation was shown to be effective for reduced representation of random fields [49] and design optimization under uncertainty [45], the overall computational cost (while linear in the dimension) can be further reduced.

The main contribution of the paper is a novel algorithm that efficiently and simultaneously computes the basis rotation as well as the corresponding chaos coefficients using a fixed number of model evaluations independent of the choice of reduced dimensionality, and as a result departing from the restrictive traditional pseudo-spectral approaches. This is achieved by incorporating an ℓ_1 -minimization procedure on Hermite Chaos expansions with respect to variables that are assumed to be orthogonal projections of the original input variables through a projection map that is computed jointly with the ℓ_1 -minimization. The advantages of our algorithm is highlighted on an example of extreme scale computation for a realistic engineering application, involving large-eddy simulations (LES) of supersonic turbulent reactive flows inside a scramjet engine combustor, where the input space is high dimensional and a very limited number of these expensive simulations is available.

This paper is structured as follows. Section 2.1 describes the use of PC expansion as a response surface, including Hermite (Homogeneous) Chaos for both standard Gaussian variables and rotated Gaussian variables produced from the basis adaptation procedure. Section 2.2 provides the main ingredients of compressive sensing, which are combined with basis adaptation to estimate the new expansion coefficients. The overall method is then demonstrated on a series of numerical examples in Section 3, including a 12-dimensional ridge function, a 20-dimensional Burgers' equation, and an 11-dimensional scramjet combustor application. The paper then ends with conclusions in Section 4.

2. Methodology

2.1. Polynomial Chaos Expansion

2.1.1. Homogeneous Chaos

Throughout this paper, let us assume the quantity

$$u := u(\boldsymbol{\xi}), \quad (1)$$

that can be written as a function of uncorrelated Gaussian variables $\boldsymbol{\xi} = (\xi_1, \dots, \xi_d)$, is a square integrable function, that is $u \in L^2(\Omega, \mathcal{F}, \mathbb{P})$, where $\mathcal{F} := \mathcal{F}(\mathcal{G})$ is the σ -algebra generated from the Gaussian Hilbert space $\mathcal{G} = \text{span}\{\xi_i\}_{i=1}^d$. It is known [51, 5, 22] that u admits a series expansion of the form

$$u(\boldsymbol{\xi}) = \sum_{\boldsymbol{\alpha}, |\boldsymbol{\alpha}|=0}^{\infty} c_{\boldsymbol{\alpha}} \psi_{\boldsymbol{\alpha}}(\boldsymbol{\xi}), \quad (2)$$

where $\boldsymbol{\alpha} = (\alpha_1, \dots, \alpha_d) \in \mathcal{J}^d := \mathbb{N}^d \cup \{\mathbf{0}\}$ are finite-dimensional multiindices with norm $|\boldsymbol{\alpha}| = \alpha_1 + \dots + \alpha_d$, and the basis functions $\psi_{\boldsymbol{\alpha}}$ are defined as the tensor product

$$\psi_{\boldsymbol{\alpha}}(\boldsymbol{\xi}) = \prod_{i=1}^d \psi_{\alpha_i}(\xi_i) \quad (3)$$

with

$$\psi_n(\xi) = \frac{h_n(\xi)}{\sqrt{n!}} \quad (4)$$

and h_n is the standard 1-dimensional Hermite polynomials of order n which is orthogonal with respect to the Gaussian measure with density $p(\xi) = (2\pi)^{-1/2} \exp(-\xi^2/2)$ and has norm $\|h_n\| = 1$, $n \in \mathbb{N}$. The Hilbert structure of $L^2(\Omega, \mathcal{F}, \mathbb{P})$ is characterized by the inner product defined as

$$\langle \psi_{\boldsymbol{\alpha}}(\boldsymbol{\xi}), \psi_{\boldsymbol{\beta}}(\boldsymbol{\xi}) \rangle := \mathbb{E} \{ \psi_{\boldsymbol{\alpha}} \psi_{\boldsymbol{\beta}} \} = \int_{\mathbb{R}^d} \psi_{\boldsymbol{\alpha}}(\boldsymbol{\xi}) \psi_{\boldsymbol{\beta}}(\boldsymbol{\xi}) p(\boldsymbol{\xi}) d\boldsymbol{\xi} \quad (5)$$

where $p(\boldsymbol{\xi}) = \prod_{i=1}^d p(\xi_i)$, $\|\psi_{\boldsymbol{\alpha}}\| = (\mathbb{E}\{\psi_{\boldsymbol{\alpha}}^2\})^{1/2}$, thus the orthogonality condition is given by

$$\langle \psi_{\boldsymbol{\alpha}}(\boldsymbol{\xi}), \psi_{\boldsymbol{\beta}}(\boldsymbol{\xi}) \rangle = \|\psi_{\boldsymbol{\alpha}}\|^2 \delta_{\boldsymbol{\alpha}, \boldsymbol{\beta}}, \quad (6)$$

where $\delta_{\boldsymbol{\alpha}, \boldsymbol{\beta}}$ is the Dirac delta function taking the value of 1 if $\boldsymbol{\alpha} = \boldsymbol{\beta}$ and 0 otherwise. Eq. (4) suggests that $\|\psi_{\boldsymbol{\alpha}}\| = 1$, and so the polynomials are normalized. We refer to Eq. (2) as the *polynomial chaos expansion* of u .

In practice, we work with truncated versions of (2). For $Q \in \mathbb{N}$, $\mathcal{J}_Q^d := \{\boldsymbol{\alpha} \in \mathcal{J}^d : |\boldsymbol{\alpha}| \leq Q\}$, we assume that u can be *accurately* approximated by

$$u(\boldsymbol{\xi}) \approx \sum_{\boldsymbol{\alpha} \in \mathcal{J}_Q^d} c_{\boldsymbol{\alpha}} \psi_{\boldsymbol{\alpha}}(\boldsymbol{\xi}). \quad (7)$$

This truncated expansion of order Q consists of

$$N_Q = \binom{d+Q}{Q} = \frac{(d+Q)!}{d!Q!} \quad (8)$$

basis terms whose coefficients $\{c_{\boldsymbol{\alpha}}\}_{\boldsymbol{\alpha} \in \mathcal{J}_Q^d}$ need to be computed.

2.1.2. Adaptation on the Gaussian basis

From the above, it is clear that all u that are \mathcal{F} -measurable can be expressed as a function of any basis of \mathcal{G} . This encompasses any set of uncorrelated standard normal random variables that spans \mathcal{G} , since the latter generates identical Chaos spaces of higher order. Assume $\mathbf{A} : \mathbb{R}^d \rightarrow \mathbb{R}^d$ is a unitary matrix ($\mathbf{A}\mathbf{A}^T = \mathbf{I}$) that serves as a linear operator from \mathbb{R}^d to itself, and taking $\boldsymbol{\xi}$ to be an *initially* chosen basis, then

$$\boldsymbol{\eta} = \mathbf{A}\boldsymbol{\xi} \quad (9)$$

defines a new set of independent standard normal random variables that spans \mathcal{G} , and therefore generating the same σ -algebra $\mathcal{F}(\mathcal{G})$. As a result, any $u \in L^2(\Omega, \mathcal{F}, \mathbb{P})$ can also be expanded as

$$u := u(\boldsymbol{\eta}) = \sum_{\boldsymbol{\beta} \in \mathcal{J}_Q^d} \tilde{c}_{\boldsymbol{\beta}} \psi_{\boldsymbol{\beta}}(\boldsymbol{\eta}) = \sum_{\boldsymbol{\beta} \in \mathcal{J}_Q^d} \tilde{c}_{\boldsymbol{\beta}} \psi_{\boldsymbol{\beta}}(\mathbf{A}\boldsymbol{\xi}) \quad (10)$$

where from the almost sure equality $u(\boldsymbol{\xi}) \stackrel{\text{a.s.}}{=} u(\boldsymbol{\eta})$ we have that

$$c_{\boldsymbol{\alpha}} = \sum_{\boldsymbol{\beta} \in \mathcal{J}_Q^d} \tilde{c}_{\boldsymbol{\beta}} \langle \psi_{\boldsymbol{\beta}}(\mathbf{A}\boldsymbol{\xi}), \psi_{\boldsymbol{\alpha}}(\boldsymbol{\xi}) \rangle. \quad (11)$$

Of high interest is the \mathbf{A} that leads to an expansion of $u(\boldsymbol{\eta})$ (for a given fixed order Q) that depends primarily only on a small number of components. In other words, we would like to construct $\tilde{\boldsymbol{\eta}} = (\eta_1, \dots, \eta_{d_0})^T$ with $d_0 \ll d$ such that

$$u(\boldsymbol{\xi}) \approx u(\tilde{\boldsymbol{\eta}}) = u(\mathbf{W}\boldsymbol{\xi}) = \sum_{\gamma \in \mathcal{J}_Q^{d_0}} \tilde{c}_\gamma \psi_\gamma(\mathbf{W}\boldsymbol{\xi}), \quad (12)$$

where the coefficients of the terms $\psi_\gamma(\boldsymbol{\eta})$ for $\gamma \in \mathcal{J}_Q^d \setminus \mathcal{J}_Q^{d_0}$ are assumed to take small values and therefore can be neglected. Here, \mathbf{W} is the matrix from decomposing the isometry

$$\mathbf{A} = \begin{bmatrix} \mathbf{W} \\ \mathbf{V} \end{bmatrix} \quad (13)$$

where $\mathbf{W}^T \in \mathcal{M}_{d_0}^d$, $\mathbf{V}^T \in \mathcal{M}_{d-d_0}^d$ with \mathcal{M}_m^n being the set of $n \times m$ matrices with orthogonal columns

$$\mathcal{M}_m^n = \{\mathbf{U} \in \mathbb{R}^{n \times m} : \mathbf{U}^T \mathbf{U} = \mathbf{I}_m\}, \quad (14)$$

and is also known as the *Stiefel manifold* [50].

Several criteria for choosing the isometry \mathbf{A} have been proposed in [47], but relying on knowing either the QoI cumulative distribution function or its low (e.g., first or second) order PC coefficients in a $\boldsymbol{\xi}$ -expansion. Both approaches require prior computations to construct \mathbf{A} , which do not provide information on the reduced dimensionality d_0 , and can be computationally inefficient as they are mainly associated with non-intrusive pseudo-spectral methods. Our goal is to develop a novel way of simultaneously computing optimal projection matrices and estimating the resulting expansion coefficients, with the flexibility of utilizing non-structured samples instead of quadrature nodes.

2.2. Compressive Sensing

2.2.1. ℓ_1 -minimization for polynomial regression

To estimate the chaos coefficients $\mathbf{c} = \{c\}_{\alpha \in \mathcal{J}_Q}$, we employ compressive sensing (CS) techniques [6, 13] that seek sparse PC representations. CS is particularly advantageous for scenarios where \mathbf{c} is indeed sparse, $\boldsymbol{\xi}$ is high-dimensional, and a very limited number of model evaluations are available. These methods make use of the fact that a PC expansion is linear with respect to its coefficients:

$$\mathbf{u} \approx \Psi \mathbf{c}, \quad (15)$$

where $\mathbf{u} = (\hat{u}^{(1)}, \dots, \hat{u}^{(N)})^T$ is the vector of output data, $\{\boldsymbol{\xi}^{(i)}\}_{i=1}^N$ is the set of input points corresponding to the data outputs, and Ψ is the measurement matrix with entries $(\Psi)_{ij} = \psi_j(\boldsymbol{\xi}^{(i)})$, $i = 1, \dots, N$, $j \in \mathcal{J}_Q^d$. We also denote the full dataset with $\mathcal{D} = \left\{ \{\boldsymbol{\xi}^{(i)}\}_{i=1}^N, \{\hat{u}^{(i)}\}_{i=1}^N \right\}$, that is the set of all available data points. In practice, as we will see next, the training data, that is the data points used to infer any parameters of interest, will be either \mathcal{D} or a subset of it. The influence of the coefficients is typically observed to quickly decay with higher order polynomials, an effect that makes the ℓ_1 -minimization a suitable method when one is interested in obtaining a sparse solution.

We focus on the following form of ℓ_1 -minimization:

$$\mathcal{P}_{1,\epsilon} := \left\{ \arg \min_{\mathbf{c}} \|\mathbf{c}\|_1 \quad s.t. \quad \|\mathbf{u} - \Psi \mathbf{c}\|_2 \leq \epsilon \right\}. \quad (16)$$

The $\mathcal{P}_{1,\epsilon}$ problem is known as the Basis Pursuit Denoising problem. When $\epsilon = 0$ is chosen to enforce an exact fit on the data, it is known as Basis Pursuit problem. Equivalence with the Least Absolute Shrinkage Operator (LASSO) [46] problem can also be shown under proper choices of the regularization and tolerance parameters [14].

2.2.2. Cross validation for choosing ϵ

In order to obtain a solution for the $\mathcal{P}_{1,\epsilon}$ problem that is useful for subsequent predictions, one needs to choose $\epsilon > 0$ properly to avoid overfitting or underfitting the data. Small values of ϵ might result in overfitting the training data without necessarily providing accurate predictions on points outside the training set. Large values of ϵ on the other hand will penalize heavily on the sparsity of the solution without taking into account the observations. We use cross-validation to find a suitable choice of ϵ . We divide the N observations into two sets consisting of N_{tr} and N_v samples ($N = N_r + N_v$) that will serve as the training and validation data respectively and we denote with Ψ_{tr} and Ψ_v the corresponding measurement matrices. We solve $\mathcal{P}_{1,\epsilon}$ using only the N_{tr} training data points and for a discrete set of values ϵ_{tr} to obtain \mathbf{c}_{tr} . For each solution we compute the validation error $\epsilon_v = \|\mathbf{u}_v - \Psi_v \mathbf{c}_{tr}\|_2$ and choose ϵ_{tr} such that ϵ_v is minimized. The procedure is summarized in Algorithm 1. Alternative cross validation procedures that can be preferable particularly in large datasets involve partitioning the data into K sets (folds), that each consists of $n_k = N/K$ points and repeating the above procedure K times where each time one fold serves as the validation set while the remaining points are the training set (leave- n_k -out cross validation) [28, 27], however, such procedures are beyond our scope.

Algorithm 1: Cross validation algorithm for estimation of ϵ

Arbitrarily choose N_{tr} out of N data points in \mathcal{D} , denote it with \mathcal{D}_{tr} and set $\mathcal{D}_v = \mathcal{D} \setminus \mathcal{D}_{tr}$. Choose a span of J values $\{\epsilon_{tr}^j\}$, $j = 1, \dots, J$

for $j = 1$ **to** J **do**

$\mathbf{c}_{tr} \leftarrow$ Solution of $\mathcal{P}_{1,\epsilon_{tr}^j}$ using data \mathcal{D}_{tr}

 Compute $\epsilon_v^j = \|\mathbf{u}_v - \Psi_v \mathbf{c}_{tr}\|_2$.

end

Return $\epsilon = \sqrt{\frac{N}{N_{tr}}} \epsilon^*$ where $\epsilon^* = \min_j \epsilon_v^j$.

In the above algorithm note that the $\sqrt{\frac{N}{N_{tr}}}$ scaling is motivated by the fact that *the validation error on the validation samples becomes large as the values of ϵ_{tr} increase, while it is smaller than the error $\|\mathbf{u} - \Psi \mathbf{c}_{tr}\|_2$ when using the full set \mathcal{D} [16].*

2.2.3. ℓ_1 -minimization using adapted PCE

Assuming now that the observed model output admits a representation of the form (12), one might be interested in finding the *best* projection matrix \mathbf{W} such that the observed data can be explained as emerging from a d_0 -dimensional PC expansion over polynomials of $\tilde{\boldsymbol{\eta}}$, for a given $d_0 \ll d$. The linear model in this case is written as

$$\mathbf{u} \approx \Psi_{\mathbf{W}} \mathbf{c}. \quad (17)$$

Here \mathbf{u} and \mathbf{c} are as in (16) while the measurement matrix has entries $(\Psi_{\mathbf{W}})_{ij} = \psi_j(\tilde{\boldsymbol{\eta}}^{(i)})$, where $\tilde{\boldsymbol{\eta}}^{(i)} = \mathbf{W} \boldsymbol{\xi}^{(i)}$, $i = 1, \dots, N$, $j \in \mathcal{J}_Q^{d_0}$. The ℓ_1 -minimization problem can be restated as

$$\mathcal{P}_{1,\epsilon}^{\mathbf{W}} := \left\{ \arg \min_{\mathbf{c}} \|\mathbf{c}\|_1 \quad s.t. \quad \|\mathbf{u} - \Psi_{\mathbf{W}} \mathbf{c}\|_2 \leq \epsilon \right\} \quad (18)$$

where with $\mathcal{P}_{1,\epsilon}^{\mathbf{W}}$ we emphasize the dependence of the solution on the projection matrix \mathbf{W} .

In practice, the projection matrix is not known a priori and needs to be estimated using a criterion that will guarantee some sense of optimality. Provided that all we have available is the data set \mathcal{D} , a natural choice is to minimize the ℓ_2 error of the model fit to the data, that is to solve

$$\mathbf{W}^* = \arg \min_{\mathbf{W}: \mathbf{W}^T \in \mathcal{M}_{d_0}^d} \|\Psi_{\mathbf{W}} \mathbf{c} - \mathbf{u}\|_2, \quad (19)$$

where \mathbf{W} appears only in the measurement matrix $\Psi_{\mathbf{W}}$ and we assume that a candidate for \mathbf{c} (e.g., an initial guess) is available. This motivates an iterative procedure, to be described in the next section. To further

justify our choice, it can be easily shown that this criterion is equivalent to the maximum likelihood estimate in the Bayesian context [42]. We emphasize that the above is a constrained optimization problem since the unknown parameters are required to satisfy the orthonormality conditions; in other words, the solution is restricted within the Stiefel manifold $\mathcal{M}_{d_0}^d$.

2.2.4. Computational algorithm

We have described the ℓ_1 -minimization problem for adapted PC expansions that requires knowledge of \mathbf{W} , while the estimation of \mathbf{W} requires the knowledge of \mathbf{c} . In what follows, we propose a two-step optimization scheme that can address the challenge of solving this coupled optimization problem. The algorithm is simply based on the heuristic idea that the two optimization problems can be interchangeably solved such that the solution of the one is kept fixed while solving the other, until some convergence criterion is satisfied. The pseudocode for this idea is summarized in Algorithm 2.

Algorithm 2: Compressive sensing with built-in basis adaptation

Require: Observed inputs $\{\boldsymbol{\xi}^{(i)}\}_{i=1}^N$, observed outputs $\{u^{(i)}\}_{i=1}^N$, choice of $d_0 < d$, initial guess $\mathbf{c}^0 \in \mathbb{R}^{|\mathcal{J}_Q^{d_0}|}$, $\mathbf{W}^0 \in \mathcal{M}_{d_0}^d$, maximum number of iterations M_{iter} , convergence tolerances ϵ_{ℓ_1} and ϵ_l , fitting error ϵ . Set $it = 1$.

repeat

Compute $\{\boldsymbol{\eta}^{(i)}\}_{i=1}^N$ and $\Psi_{\mathbf{W}^{it-1}}$ where $\boldsymbol{\eta}^{(i)} = \mathbf{W}^{it-1}\boldsymbol{\xi}^{(i)}$, $i = 1, \dots, N$ and $[\Psi_{\mathbf{W}^{it-1}}]_{kl} = \psi_l(\boldsymbol{\eta}^{(k)})$
 $\mathbf{c}^{it} \leftarrow \arg \min_{\mathbf{c}} \|\mathbf{c}\|_1$ subject to $\|\mathbf{u} - \Psi_{\mathbf{W}^{it-1}}\mathbf{c}\|_2 < \epsilon$
 $\mathbf{W}^{it} \leftarrow \arg \min_{\mathbf{W}} \|\mathbf{u} - \Psi_{\mathbf{W}}\mathbf{c}^{it}\|_2^2$
 $it \leftarrow it + 1$

until relative change in $\|\mathbf{c}\|_1$ is less than ϵ_{ℓ_1} and change in $\mathcal{F}(\mathbf{W})$ is less than ϵ_l or $it = M_{iter}$

While the proposed algorithm involves iterating between two tractable subproblems (ℓ_1 and ℓ_2 -minimizations), it does not address how to choose d_0 , and the issue of increasing dimensionality of both arguments \mathbf{c} and \mathbf{W} when one increases d_0 . More specifically, upon solving (18) for a small value d_0 , one may decide that the resulting PC expansion is not accurate enough, and therefore, the need to increase d_0 and repeat the procedure. The number of expansion coefficients increases factorially with d_0 while the number of entries in \mathbf{W} increases geometrically, and the combined effect can result in an expensive-to-solve problem as we move to larger d_0 values. In practice, the growth mainly affects the constrained optimization problem with respect to \mathbf{W} , and the convergence to a global minimum can become slow.

Another drawback of the proposed procedure is the possibility to be stuck in a local minimum. This is mainly due to the fact that the objective function to be optimized with respect to \mathbf{W} is generally non-convex. In addition, it can be observed that for a given d_0 , the optimal solution provides a PC expansion with respect to a germ $\boldsymbol{\eta}$ that can itself be rotated along the d_0 -dimensional space, resulting in an infinite number of possible expansions that are almost surely equal and with the same ℓ_2 value, while the ℓ_1 norms of the chaos coefficients are not necessarily equal. This property is further explained in Appendix B. As a result, the algorithm might not converge to the globally maximum likelihood when minimizing with respect to \mathbf{W} ,

In order to reduce the number of parameters in our optimization problem, and thus improve its efficiency, we also propose a second algorithm that computes the rows of \mathbf{W} by successively solving the optimization problem with respect to each row at a time while fixing the entries of the rows that have already been estimated; the pseudocode is presented in Algorithm 3. This algorithm replaces the problem of minimizing the ℓ_2 error with respect to $d_0 \times d$ parameters with that of solving d_0 minimization problems with d parameters each time (note that the increase of the number of chaos coefficients at each problem does not add up significant computational complexity) To further ensure convergence to the global minimum, we repeat the procedure multiple times from different initial conditions and select the solution corresponding to the lowest minimum. At small values of d' , it is possible that the linear system is overdetermined and ordinary least squares (OLS) can be employed instead of $\mathcal{P}_{1,\epsilon}$. One can therefore replace the corresponding

step with an OLS solution until the problem becomes underdetermined as d' is increased. Both approaches are expected to perform similarly as the $\mathcal{P}_{1,\epsilon}$ solution tends toward the OLS solution for large values of N .

Algorithm 3: Successive row estimation of the projection matrix

Require : Observed inputs $\{\boldsymbol{\xi}^{(i)}\}_{i=1}^N$, observed outputs $\{u^{(i)}\}_{i=1}^N$, choice of $1 < d_0 < d$, initial guess $\mathbf{c}^0 \in \mathbb{R}^{|\mathcal{J}_Q^1|}$, $\mathbf{w}^0 \in \mathcal{M}_1^d$, maximum number of iterations M_{iter} , convergence tolerances ϵ_{ℓ_1} and ϵ_l , fitting error ϵ .

Initialize: Set $d' = 1$ and use Algorithm 2 to solve (18) and obtain $\mathbf{W}^* \in \mathcal{M}_1^d$ and $\mathbf{c}^* \in \mathbb{R}^{|\mathcal{J}_Q^1|}$.

for $d' = 2$ to d_0 **do**

· Set $\mathbf{W}^{d'} = \mathbf{W}^*$.

· Generate random initial guess $\mathbf{c}^0 \in \mathbb{R}^{|\mathcal{J}_Q^{d'}|}$, $\mathbf{w}^0 \in \mathcal{M}_1^d$ such that $\mathbf{W}^{d'} \cdot \mathbf{w}^{0T} = \mathbf{0} \in \mathbb{R}^{d'-1}$ and set $\mathbf{W}^0 = [\mathbf{W}^{d'T} \ \mathbf{w}^{0T}]^T$

· Employ Algorithm 2 to obtain new $\mathbf{W}^* \in \mathcal{M}_d^d$, and $\mathbf{c}^* \in \mathbb{R}^{d'}$ while the first $d' - 1$ rows of \mathbf{W}^* are kept fixed (and equal to $\mathbf{W}^{d'}$).

end

3. Examples

A set of numerical examples are presented below to demonstrate the performance of our methodology. The algorithm is validated in Sec. 3.1 on a synthetic example where the exact adaptation and solutions are known. In Sec. 3.2, the technique is applied on a high-dimensional benchmark UQ problem: the stochastic Burgers' equation with a 20-dimensional random forcing term. We compare two cases where the first has a relatively benign random forcing with decaying amplitudes, and the other has non-decaying amplitudes to further challenge our algorithm. We end this section with a realistic engineering application involving LES of turbulent reactive flows in a scramjet engine combustor (Sec. 3.3), where engine performance QoIs are functions of 11 uncertain input parameters, and a full-dimensional chaos expansion would be infeasible due to the computational requirements of the simulations.

For the ℓ_1 -minimization, we employ the Douglas-Rachford algorithm [17, 8] that is a splitting technique of finding a zero of the sum of two maximally monotone operators. For the optimization with respect to the projection matrix subject to orthogonality constraints, we make use of the Sequential Quadratic Programming (SQP) algorithm ([33], Ch. 18) that solves a sequence of subproblems that optimize a quadratic model of the objective function. SQP requires knowledge of the gradients of the objective function which are derived in Appendix A. Another alternative for optimization problems with orthogonal constraints would be to follow a Crank-Nicolson-like update scheme [48]. However, our implementations primarily focus on Algorithm 3 which involves optimization with respect to one matrix row at a time, and we do not pursue extensive exploration of more sophisticated optimization algorithms at this time.

3.1. Ridge function with known adaptation

We consider the function $u : \mathbb{R}^d \rightarrow \mathbb{R}$ that is given by

$$u(\boldsymbol{\xi}) = \sum_{i=1}^d \xi_i + 0.25 \left(\sum_{i=1}^d \xi_i \right)^2 + 0.025 \left(\sum_{i=1}^d \xi_i \right)^3 \quad (20)$$

which is a PC expansion due to its polynomial form, and the coefficients can easily be identified. Since $\sum_{i=1}^d \xi_i$ is a zero-mean Gaussian with variance equal to d , the above expression can be rewritten as a function of the transformed standard Gaussian variable

$$\eta_1 = d^{-1/2} \sum_{i=1}^d \xi_i, \quad (21)$$

resulting in

$$\begin{aligned} u(\eta_1) &= d^{1/2}\eta_1 + 0.25d\eta_1^2 + 0.025d^{3/2}\eta_1^3 \\ &= c_0 + c_1\psi_1(\eta_1) + c_2\psi_2(\eta_1) + c_3\psi_3(\eta_1), \end{aligned} \quad (22)$$

where

$$\mathbf{c} = \begin{pmatrix} c_0 \\ c_1 \\ c_2 \\ c_3 \end{pmatrix} = \begin{pmatrix} 0.25 \\ d^{1/2} + 0.075d^{3/2} \\ \frac{0.25d}{\sqrt{2}} \\ \frac{0.025d^{3/2}}{\sqrt{3!}} \end{pmatrix}. \quad (23)$$

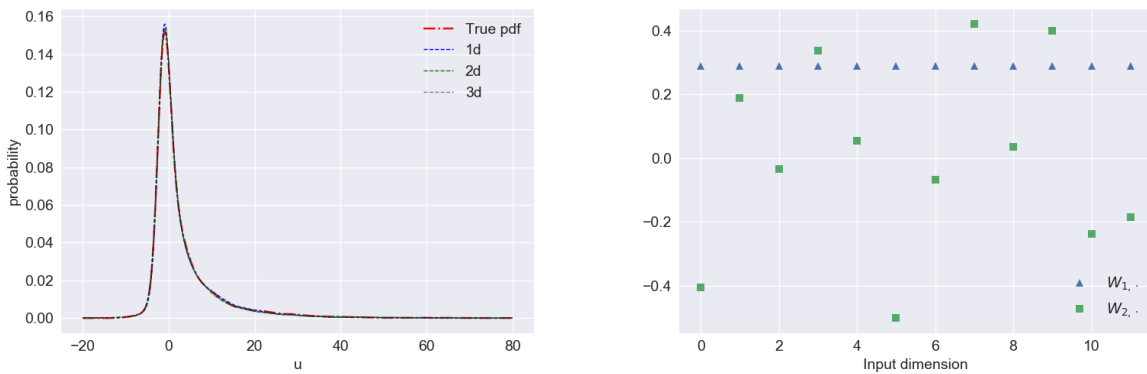


Figure 1: Left: Plots of the density functions of the true QoI along with the 1-, 2- and 3-dimensional adapted chaos approximations. Right: Values of the first two rows ($\mathbf{W}_{1,\cdot}$ and $\mathbf{W}_{2,\cdot}$) of the projection matrix, estimated using Alg. 3.

We set $d = 12$, therefore $|\mathcal{J}_3^{12}| = 455$ and we construct synthetic data that consists of $N = 180$ Monte Carlo samples ($N/|\mathcal{J}_3^{12}| \approx 0.4$). We execute Algorithm 3 and obtain the solutions for 1d, 2d, and 3d expansions. Fig. 1 shows all three density functions (left) and isometry values for the 1d and 2d cases (right). It is clear that the densities coincide since $u(\boldsymbol{\xi})$ can be written as a univariate function. The first row of the isometry is indeed as in (21) while the values of the second row are in fact insignificant since the series coefficients that correspond to η_2 (and cross terms) are zero. Fig. 2 shows the plot of a u as a function of η_1 (left) and as a bivariate function of (η_1, η_2) (right). Since the coefficients corresponding to η_2 are zero, the function exhibits no variation along η_2 . Fig. 3 shows the bivariate (2d) expansions obtained after performing 10 independent runs of Algorithm 2 and a comparison of one run from each algorithm. Interestingly we observe that at each run, Algorithm 2 converges to an arbitrary rotation and the corresponding coefficients result in an expansion $u(\eta'_1, \eta'_2)$ that itself is a rotation of $u(\eta_1, \eta_2)$ obtained by Algorithm 3. That is due to the fact that the observations incorporated in the ℓ_2 error term are each time mapped to different rotated inputs. Thus both algorithms capture the same PC expansion but Alg. 2 fails to detect a dominant direction.

3.2. Stochastic Burgers' equation

Let us consider the following initial boundary value problem (IBVP):

$$\begin{cases} \frac{\partial v}{\partial t} + v \frac{\partial v}{\partial x} = \nu \frac{\partial^2 v}{\partial x^2} + \sigma \sum_{l=1}^M \xi_l \phi_l(x, t), & x \in [0, 2\pi], \quad t \in [0, 1] \\ v(x, 0) = 1 + \sin(2x) \\ v(0, t) = v(2\pi, t) = 1 + \sin(\pi t) \end{cases} \quad (24)$$

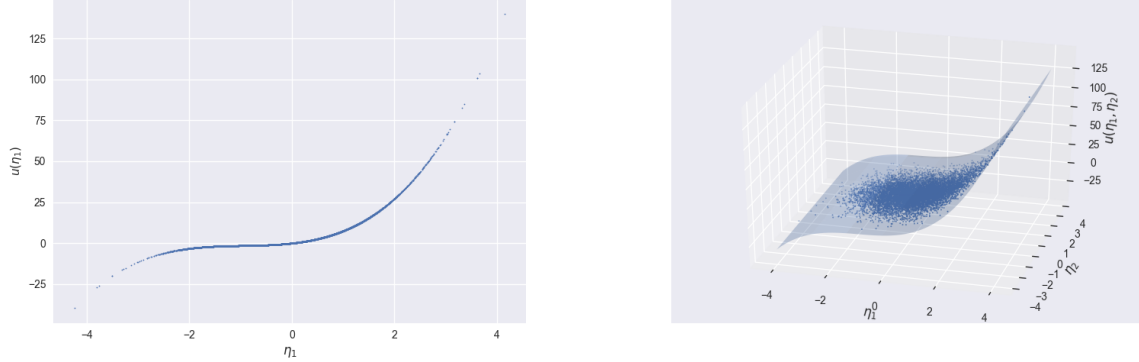


Figure 2: Plot of the QoI as a function of its 1d and 2d inputs (left and right respectively).

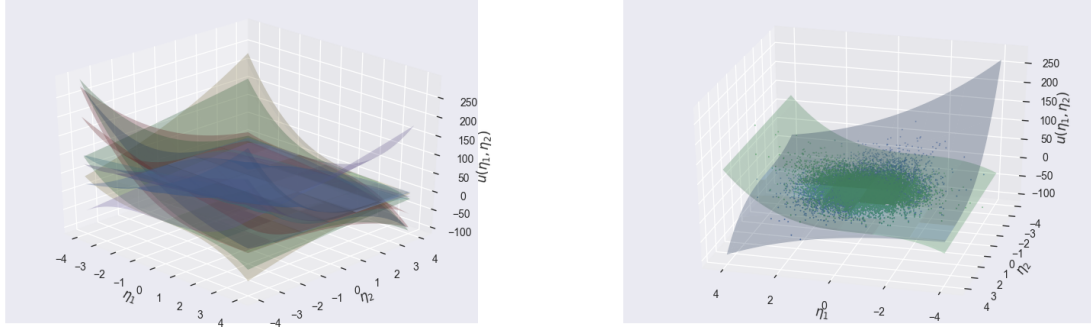


Figure 3: Left: Bivariate PC expansions obtained from 10 runs of Algorithm 2 with random initial point. Right: Comparison of a single run with the output of Algorithm 3.

where ξ_l , $l = 1, \dots, M$ are i.i.d. standard normal random variables. For the random forcing term we consider two cases: (i) $\phi_l(x, t) = \cos(2lx) \cos(2l\pi t) / \sqrt{l}$ where the strength of the random Gaussians decays as a function of l and (ii) $\psi_l(x, t) = \cos(2lx) \cos(2l\pi t) / M$ where all terms contribute equally although their coefficients maintain varying (increasing) frequencies. For our numerical implementations below we discretize $[0, 2\pi] \times [0, 1]$ into a rectangular 500×500 grid and solve the IBVP using an implicit Newton's method. The scalar QoI which we seek to expand in a PC series with respect to $\boldsymbol{\xi} = (\xi_1, \dots, \xi_M)$ is the spatial average of the solution to the IBVP at $t = 1$,

$$u(\boldsymbol{\xi}) := \frac{1}{2\pi} \int_0^{2\pi} v(x, 1; \boldsymbol{\xi}) dx. \quad (25)$$

For both cases we take $M = 20$ with $\nu = 1/2$ and $\sigma = 2$. For case (i) we set the order of the approximating expansion to be $Q = 6$ and we generate 1000 Monte Carlo samples as our synthetic data while for (ii) we reduce the order to $Q = 3$ and the number of samples is set to 700.

Fig. 4 shows the plots of the estimated 1d and 2d expansions obtained from Algorithm 3 for the two cases. For case (i), the expansions provide a good fit the data. This can be partially explained by the fact that Q is higher but most importantly because the decay in the random forcing proportional to $1/\sqrt{l}$ quickly makes ξ_i 's insignificant, and the QoI depends on only a few inputs, thus making it easy to identify a rotation in a low dimensional space. On the contrary, in case (ii) clearly both expansions provide a quite

poor fit on the data and the need to increase d_0 is apparent. A comparison of the coefficients of the 1d and 2d expansions for (i) indicates that the polynomial terms that depend on η_1 are dominant compared to those that depend on η_2 . In addition, a look at the entries of the first row of the projection matrix for the two cases confirms our assumption above regarding the increasing significance of the ξ_i 's as we move from case (i) to case (ii). In the first, only two entries have significant amplitudes, while in the second, the values exhibit fluctuations that result in η_1 being strongly dependent on all ξ_i 's. Fig. 5 shows the density functions of the PC expansions obtained for the two cases. For (i) we compare the PC expansions of dimension up to 2 as there is no reason to pursue estimation of higher dimensional expansions. For (ii) we display the densities for expansions of dimensionality up to 10 where it is observed that no convergence is yet achieved. The coefficients of all successive PC expansions are pairwise compared in Fig. 6. We observe that by using the computed rotation found for $d' - 1$, each successive run of the algorithm for d' seems to recover the coefficients of the $d' - 1$ augmented with the additional nonzero coefficients corresponding to $\eta_{d'}$ plus cross terms. Overall, the method performs effectively in both cases, however, only in the first case we manage to obtain a reduced PC expansion that can be used as an approximation of our QoI. This is due to the different effect on the random forcing on the QoI and independent of our algorithm. Nevertheless, for the second and more challenging case we still manage to draw our conclusions at a fixed computation cost, that of performing 700 runs of the PDE solver, in contrast to using quadrature methods which would require far more model evaluations. For instance, using a level 1 quadrature rule to compute first order coefficients as in [47], and then using a level 3 (to account for $Q = 3$ in this case) quadrature rule on the reduced basis from $d_0 = 1$ up to 10, would require a total of 8501 evaluations!

3.3. Turbulent reactive flows in a scramjet engine combustor

UQ for supersonic reactive flows using large eddy simulations (LES) has only recently become feasible owing to both algorithmic advances and increasing computational power and resources. This development has allowed researchers to explore beyond the commonly used Reynolds-averaged Navier-Stokes (RANS) model [54]. Even with the use of RANS, hybrid RANS/LES, or Detached Eddy simulations (DES) [43], construction of accurate response surfaces for QoIs faces insurmountable challenges due to the large number of simulations required to explore the often high-dimensional space of uncertain model parameters. Indeed, systematic UQ studies for supersonic combustor ramjet (scramjet) engines is currently rare, with a few exceptions [52, 10]. Only very recently, CS methods were used for computation of PC surrogates for scramjet computations [27] and global sensitivity analysis studies were presented [26].

3.3.1. The model

We concentrate on a scramjet configuration studied under the HIFiRE (Hypersonic International Flight Research and Experimentation) program [11, 12], where the flight test payload (Figure 7) involves a cavity-based hydrocarbon-fueled dual-mode scramjet. A ground test rig, designated the HIFiRE Direct Connect Rig (HDCR) (7), was developed to duplicate the isolator/combustor layout of the flight test hardware [25, 44]. Mirroring the HDCR setup, we aim to simulate and assess flow characteristics inside the isolator/combustor portion of the scramjet.

We simulate reactive flows through the HDCR. The rig consists of a constant-area isolator (planar duct) attached to a combustion chamber. It includes four primary injectors that are mounted upstream of flame stabilization cavities on both the top and bottom walls. Four secondary injectors along both walls are positioned downstream of the cavities. The primary fuel injectors are located at $x = 244$ mm from the inlet and aligned at 15° from the wall, while the secondary injectors are at $x = 419$ mm and aligned at 90° from the wall. All injectors have a diameter of $d = 3.175$ mm. Flow travels from left to right in the x -direction (streamwise), and the geometry is symmetric about the centerline in the y -direction. Numerical simulations take advantage of this symmetry by considering a domain that covers only the bottom half of this configuration. To further reduce the computational cost, we consider one set of primary/secondary injectors and impose periodic conditions in the z -direction (spanwise). The overall computational domain is highlighted by the red lines in 8. JP-7 surrogate fuel [37] is inserted through these injectors, containing 36% methane and 64% ethylene by volume (mole). A reduced, three-step mechanism is employed to characterize the combustion process, and its kinetic parameters are tuned for the current simulations [29].

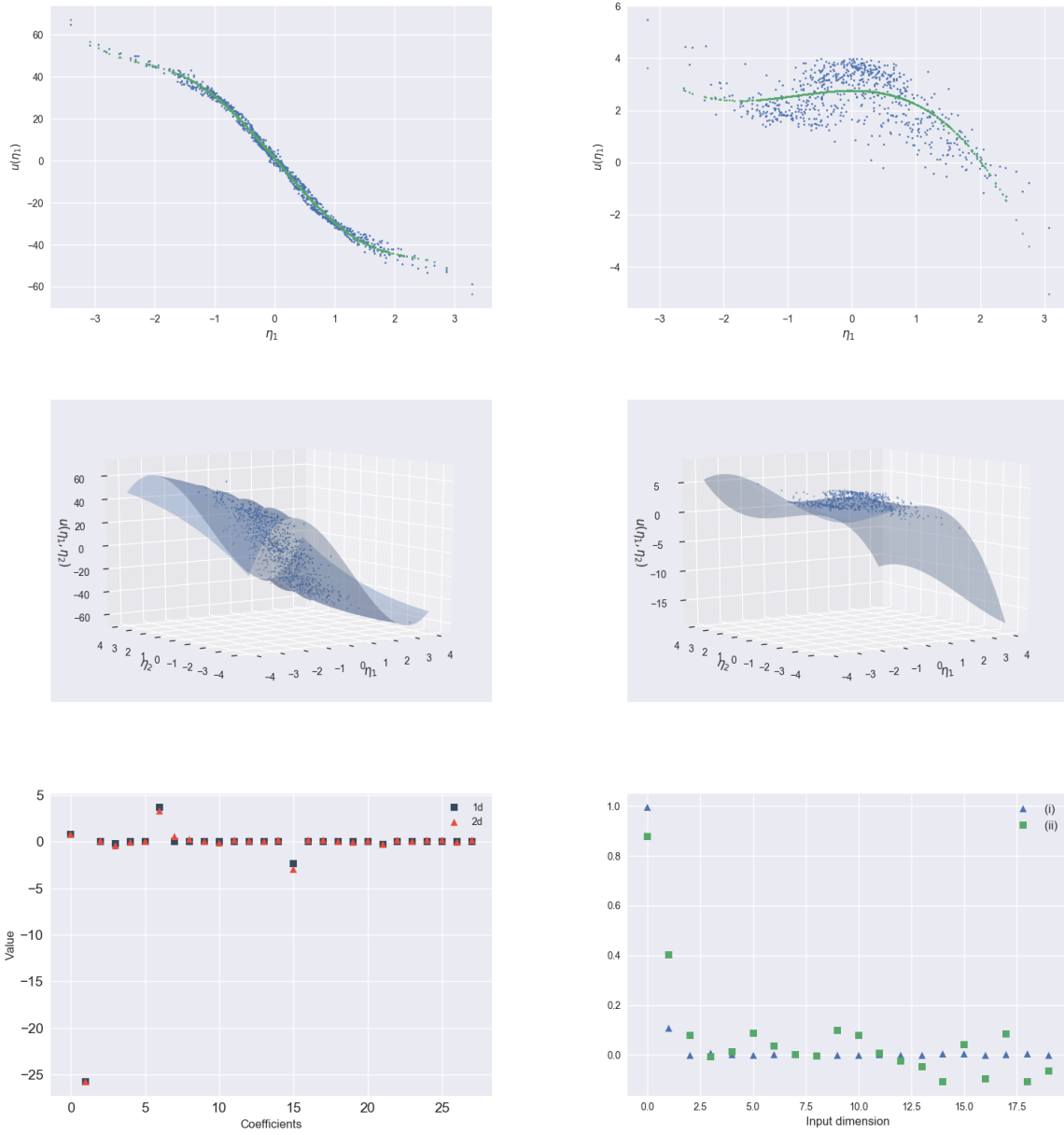


Figure 4: Top: Plot of the QoI as a function of its 1d input for case (i) (left) and case (ii) (right). Middle: Plot of the QoI as a function of its 2d input for case (i) (left) and case (ii) (right). Bottom: Coefficients of 1d and 2d expansions for case (i) (left) and comparison of the first row of \mathbf{W} for the two cases (right).

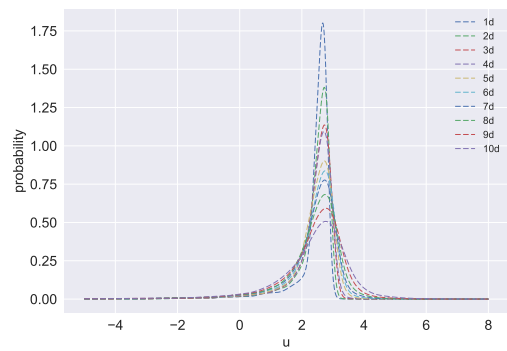
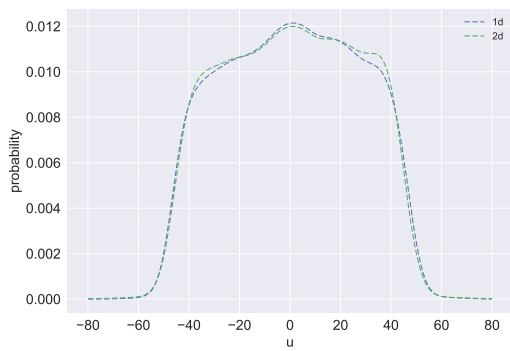


Figure 5: Density functions of the PC expansions for $d_0 = 1, 2$ in case (i) (left) and for $d_0 = 1, \dots, 10$ in case (ii) (right).

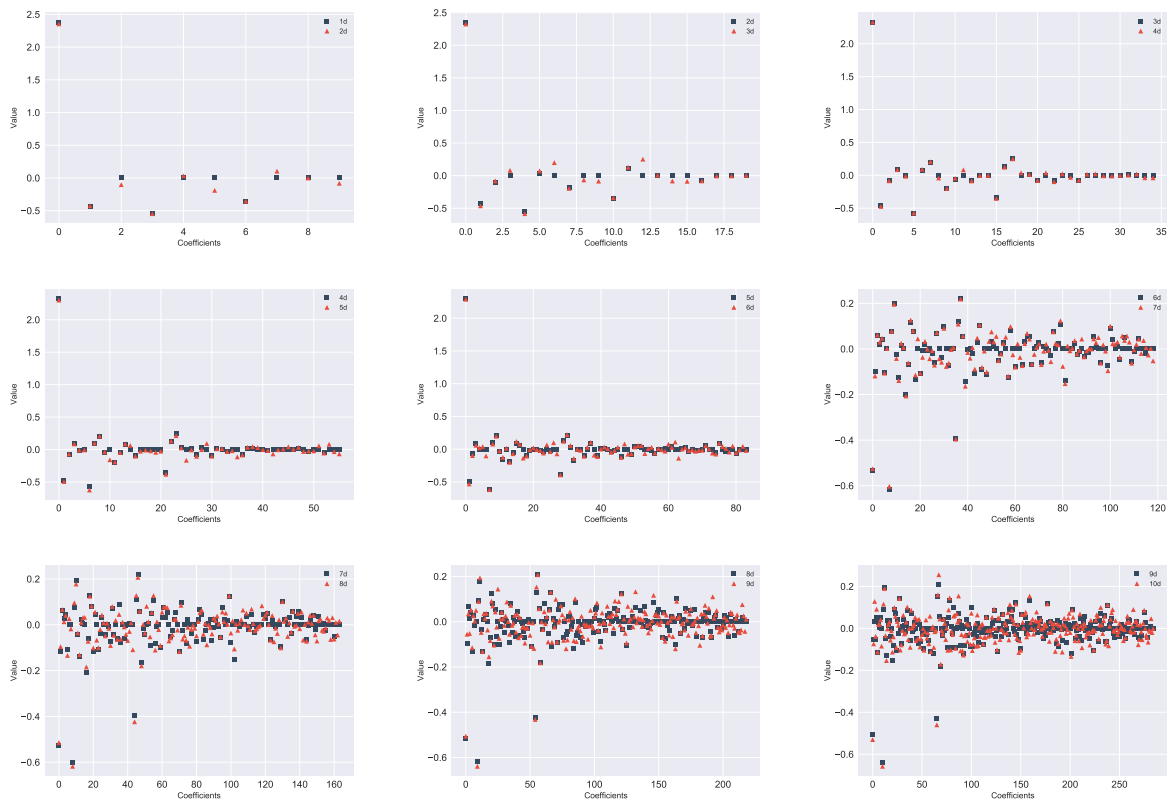


Figure 6: Case (ii): Plot of chaos coefficients for expansions with consecutive increase in dimensionality, from 1d-2d (top left) to 9d-10d (bottom right). To improve visibility along the y -axis, the zeroth order coefficient is ignored in the comparison of 6d-7d and higher orders.

LES calculations are then performed using the RAPTOR code framework developed by Oefelein [35, 34]. The solver has been optimized to meet the strict algorithmic requirements imposed by the LES formalism. The theoretical framework solves the fully coupled conservation equations of mass, momentum, total-energy, and species for a chemically reacting flow. It is designed to handle high Reynolds number, high-pressure, real-gas and/or liquid conditions over a wide Mach operating range. It also accounts for detailed thermodynamics and transport processes at the molecular level. RAPTOR employs non-dissipative, discretely conservative, staggered, finite-volume differencing, which eliminates numerical contamination due to artificial dissipation and produces high quality LES results.

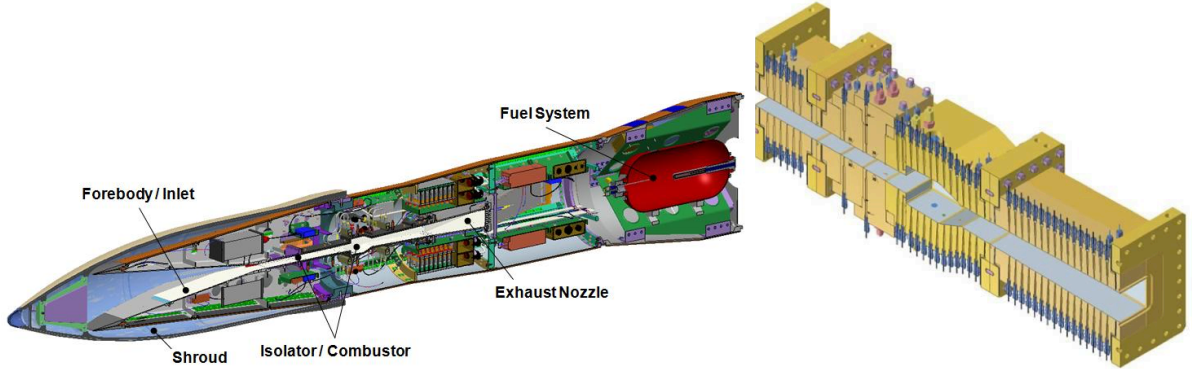


Figure 7: HIFiRE Flight 2 payload (left) and HDCR cut view (right).

3.3.2. Input parameters and quantities of interest

In our example, we allow a total of 11 input parameters to be variable and uncertain, shown in Table 1 along with the range of admissible values. Their distributions are assumed uniform across the ranges indicated and the purpose of constructing a Hermite Chaos expansion are further mapped to Gaussian variables as explained in the next section. We focus on two QoIs: (1) burned equivalence ratio (ϕ_B) and (2) stagnation pressure loss ratio ($R_{\bar{P}}$). These QoIs reflect the overall scramjet performance, and are based on time-averaged variables. The data utilized in the current analysis are from 2D simulations of the scramjet computation, using grid resolution where cell size is 1/16 of the injector diameter $d = 3.175$ mm.

- **Burned equivalence ratio** (ϕ_B) is defined to be equal to $\phi_B \equiv \phi_T \eta_c$, where ϕ_T is the total equivalence ratio imposed on the system, and η_c is the combustion efficiency based on static enthalpy quantities [44, 24]:

$$\eta_c = \frac{H(T_{\text{ref}}, Y_e) - H(T_{\text{ref}}, Y_{\text{ref}})}{H(T_{\text{ref}}, Y_{e,\text{ideal}}) - H(T_{\text{ref}}, Y_{\text{ref}})}. \quad (26)$$

Here H is the total static enthalpy, the “ref” subscript indicates a reference condition derived from the inputs, the “e” subscript is for the exit, and the “ideal” subscript is for the ideal condition where all fuel is burnt to completion. The reference condition corresponds to that of a hypothetical non-reacting mixture of all inlet air and fuel at thermal equilibrium. The numerator, $H(T_{\text{ref}}, Y_e) - H(T_{\text{ref}}, Y_{\text{ref}})$, thus reflects the global heat released during the combustion, while the denominator represents the total heat release available in the fuel-air mixture.

- **Stagnation pressure loss ratio** ($R_{\bar{P}}$) is defined as

$$R_{\bar{P}} = 1 - \frac{P_{s,e}}{P_{s,i}}, \quad (27)$$

where $P_{s,e}$ and $P_{s,i}$ are the wall-normal-averaged stagnation pressure quantities at the exit and inlet planes, respectively.

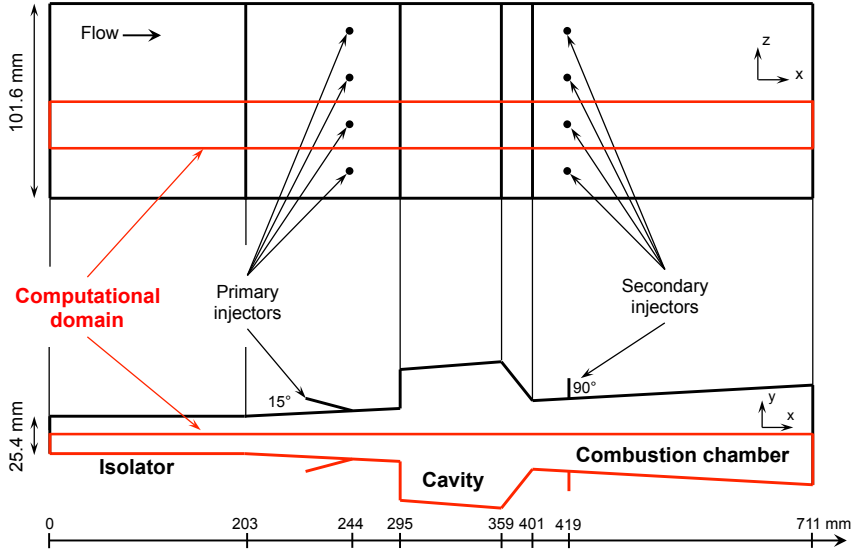


Figure 8: The HDCR experimental setup and schematic of the full computational domain.

3.3.3. Results

In order to construct Hermite Chaos expansions, we first introduce the normalized physical parameters $\theta = (\theta_1, \dots, \theta_{11}) := (\frac{\bar{p}_0}{|\bar{p}_0|}, \frac{\bar{T}_0}{|\bar{T}_0|}, \frac{\bar{M}_0}{|\bar{M}_0|}, \frac{\bar{C}_R}{|\bar{C}_R|}, \frac{\bar{Pr}_t}{|\bar{Pr}_t|}, \frac{\bar{Sc}_t}{|\bar{Sc}_t|}, \frac{\bar{I}_i}{|\bar{I}_i|}, \frac{\bar{L}_i}{|\bar{L}_i|}, \frac{\bar{R}_i}{|\bar{R}_i|}, \frac{\bar{I}_f}{|\bar{I}_f|}, \frac{\bar{L}_f}{|\bar{L}_f|})$ where $|\cdot|$ denotes the range of each parameter as that is shown in Table 1 and the bar denotes that the parameters are shifted towards zero (lower bound value is subtracted), hence all parameters are normalized to $\theta_i \in [0, 1]$. Next θ is mapped to Gaussian random germs $\xi = (\xi_1, \dots, \xi_{11})$ via the relation $\theta_i = \Phi(\xi_i)$, $i = 1, \dots, 11$ where $\Phi(\cdot)$ is the standard normal cumulative distribution function.

PC expansions of $u_1 := \phi_B$ and $u_2 := R_{\bar{P}}$ of order $Q = 4$ are constructed using Algorithm 3 for $d_0 = 1, 2, 3, 4$ and 5 on a data set consisting on 256 Monte Carlo samples, shown in Fig. 9. For each choice of d_0 and for both QoIs, it is observed that the algorithm converges to a solution after only 4-5 interchanges over the ℓ_1 -minimization procedures. In addition, for each d_0 the cross validation procedure is repeated independently in order to re-estimate ϵ and as d_0 increases the set of values ϵ_{tr}^j is upper bounded by the value chosen at $d_0 - 1$, and so the value for ϵ decreases. This agrees with intuition which suggests that by increasing the dimensionality of the adapted expansion, we should expect the fit on the data to improve.

Fig. 10 shows plots of the resulting 1D and 2D adaptations for the QoIs along with density functions of the chaos expansions up to 5D using all available observations. We observe that the computed PC expansions provide a qualitatively good fit on the observed data when the latter is plotted as function of the new rotated, reduced basis. Hence, this indicates the QoIs under consideration can be successfully represented as lower dimensional functions of the new Gaussian germs, and capture the probabilistic behavior of the full PC expansions. This is further supported by the comparison of density functions of the 5 PC expansions, which show almost identical shape for both QoIs. Fig. 11 shows the values of the first two rows of computed projection matrices that define η_1 and η_2 from ξ , for each of the QoIs. Assuming that a 1D or 2D expansion can be used as a functional representation of each QoI, these values can be used as a measure of sensitivity to each ξ_i as each of the values determines the impact of the corresponding ξ_i on the variance of η_1 and η_2 . Overall we observe that the first row values weigh the ξ_i 's in a similar way for the two QoIs. The values of the second row is slightly different for each case, however several entries maintain an agreement.

We also explore the dependence of the algorithm performance with respect to the number of data samples. Fig. 12 shows the 11 values of the projection vector \mathbf{w} for a 1D adaptation when the number of samples varies from 40 to 256 with 10-sample batch being added at a time (and 16 at the final step from 240 to 256). One can observe small fluctuations in the values when the samples vary from 40 to over 100 when they start

Table 1: Uncertain model parameters. The uncertain distributions are assumed uniform across the ranges shown.

	Notation	Range
<i>Inlet boundary conditions</i>		
Stagnation pressure	p_0	$[1.406, 1.554] \times 10^6$ Pa
Stagnation temperature	T_0	$[1472.5, 1627.5]$ K
Mach number	M_0	$[2.259, 2.761]$
Turbulence intensity horizontal component	I_i	$[0, 0.05]$
Turbulence length scale	L_i	$[0, 8] \times 10^{-3}$ m
Ratio of turbulence intensity vertical to horizontal components	R_i	$[0.8, 1.2]$
<i>Fuel inflow boundary conditions</i>		
Turbulence intensity magnitude	I_f	$[0, 0.05]$
Turbulence length scale	L_f	$[0, 1] \times 10^{-3}$ m
<i>Turbulence model parameters</i>		
Modified smagorinsky constant	C_R	$[0.01, 0.06]$
Turbulent Prandtl number	Pr_t	$[0.5, 1.7]$
Turbulent Schmidt number	Sc_t	$[0.5, 1.7]$

to converge, which suggests that the isometry could be safely recovered with about 120 samples. Next, all the computed 1D expansions are shown in Fig. 13, along with all 256 data points in order to assess the quality of the fit. Overall one can conclude that for both QoIs, even the expansions obtained with very few data points provide about the same fit on the data along the whole range of the Gaussian germ η_1 and they only start diverging from each other around the tails of the distribution that is past the $-2, 2$ values which correspond to areas where η_1 can be found with probability less than 0.05. At last, plots of the ℓ_2 residuals versus the dimensionality of the chaos expansion are shown in Fig. 14 for $N = 40, 110, 180$ and 256 verifying our initial intuition that the data fit should be improving as we move towards higher dimensions.

4. Conclusions

We presented a novel method for dimension reduction of polynomial chaos expansions by combining compressive sensing with basis adaptation. Starting with a low dimension, the new algorithm finds an optimal rotated PC expansion by alternating between two subproblems: computing the chaos coefficients via ℓ_1 -minimization, and constructing an orthogonal rotation matrix through ℓ_2 -minimization. The appropriate reduced dimension can then be selected by assessing the convergence of data fit, statistics, and distribution of the quantities of interest being represented.

The main advantage of the new method is its efficiency in estimating chaos expansions on a reduced dimension and with a usually significantly smaller number of samples compared to a full dimensional PC expansion. It also advances the basis adaptation framework by coupling it with compressive sensing algorithms thus offering flexibility to avoid the computational burden associated with the use of quadrature methods for estimation of their coefficients in pseudo-spectral approaches, particularly in high dimensions.

A promising future direction of this research would definitely involve testing its applicability to more computationally expensive or physically complex problems and to even higher dimensions. From a theoretical point of view, our methodology can be shown to be a special case of a Bayesian Compressive Sensing approach in the spirit of the work of Sargsyan [42] and our solution is the *maximum a posteriori* (MAP) estimate, corresponding to a Laplace and Uniform (on the Stiefel manifold) priors on the coefficients and the projection matrix respectively and a Gaussian Likelihood function. More general prior and likelihood function choices could lead to a more thorough understanding of the behavior of the MAP solution and the computational challenges of the algorithm. Furthermore, techniques for sampling from distributions defined on Stiefel manifolds as in [7] would enable estimation of posterior distributions of projection matrices and would be another step towards the ultimate goal that is the fully Bayesian solution of the problem.

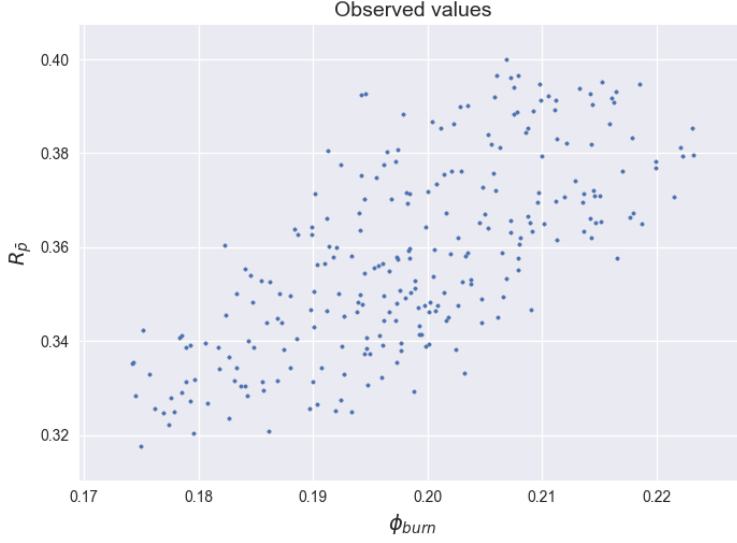


Figure 9: Set of observations of the two quantities of interest.

5. Acknowledgements

Support for this research was provided by the Defense Advanced Research Projects Agency (DARPA) program on Enabling Quantification of Uncertainty in Physical Systems (EQUiPS). Sandia National Laboratories is a multimission laboratory managed and operated by National Technology and Engineering Solutions of Sandia, LLC., a wholly owned subsidiary of Honeywell International, Inc., for the U.S. Department of Energy's National Nuclear Security Administration under contract DE-NA-0003525.

Appendix A. Gradient of the ℓ_2 error

Here we seek to derive the gradient of the ℓ_2 error function

$$\mathbf{J}(\mathbf{W}) = \|\mathbf{u} - \Psi_{\mathbf{W}}\mathbf{c}\|_2^2 = (\mathbf{u} - \Psi_{\mathbf{W}}\mathbf{c})^T (\mathbf{u} - \Psi_{\mathbf{W}}\mathbf{c}) \quad (\text{A.1})$$

with respect to the entries of \mathbf{W} . For arbitrary $\theta := (\mathbf{W})_{ij}$ we get

$$\frac{\partial \mathbf{J}(\mathbf{W})}{\partial \theta} = -2\mathbf{u}^T \frac{\partial \Psi_{\mathbf{W}}}{\partial \theta} \mathbf{c} + \mathbf{c}^T \left(\Psi_{\mathbf{W}}^T \frac{\partial \Psi_{\mathbf{W}}}{\partial \theta} + \frac{\partial \Psi_{\mathbf{W}}^T}{\partial \theta} \Psi_{\mathbf{W}} \right) \mathbf{c}. \quad (\text{A.2})$$

where $\frac{\partial \Psi_{\mathbf{W}}}{\partial \theta}$ is the matrix with entries $\frac{\partial (\Psi_{\mathbf{W}})_{k\beta}}{\partial \theta} = \frac{\partial \psi_{\beta}(\mathbf{W}\boldsymbol{\xi}^{(k)})}{\partial \theta}$. For each multi-index β and for ϵ_i being the multi-index with value 1 as its i -th entry and zero elsewhere, we have

$$\frac{\partial \psi_{\beta}(\mathbf{W}\boldsymbol{\xi})}{\partial \theta} = \sum_{r=1}^{d_0} \frac{\partial \psi_{\beta}}{\partial \eta_r} \frac{\partial \eta_r}{\partial \theta} = \frac{\partial \psi_{\beta}}{\partial \eta_i} \frac{\partial \eta_i}{\partial \theta} = \sqrt{\beta_i} \psi_{\beta - \epsilon_i}(\boldsymbol{\eta}) \xi_j \quad (\text{A.3})$$

where the last equality makes use of the fact that $\psi'_n(\eta) = \sqrt{n} \psi_{n-1}(\eta)$ and that gives

$$\frac{\partial}{\partial \eta_i} \psi_{\beta}(\boldsymbol{\eta}) = \psi'_{\beta_i}(\eta_i) \prod_{\substack{j=1 \\ j \neq i}} \psi_{\beta_j}(\eta_j) = \sqrt{\beta_i} \psi_{\beta - \epsilon_i}(\boldsymbol{\eta}). \quad (\text{A.4})$$

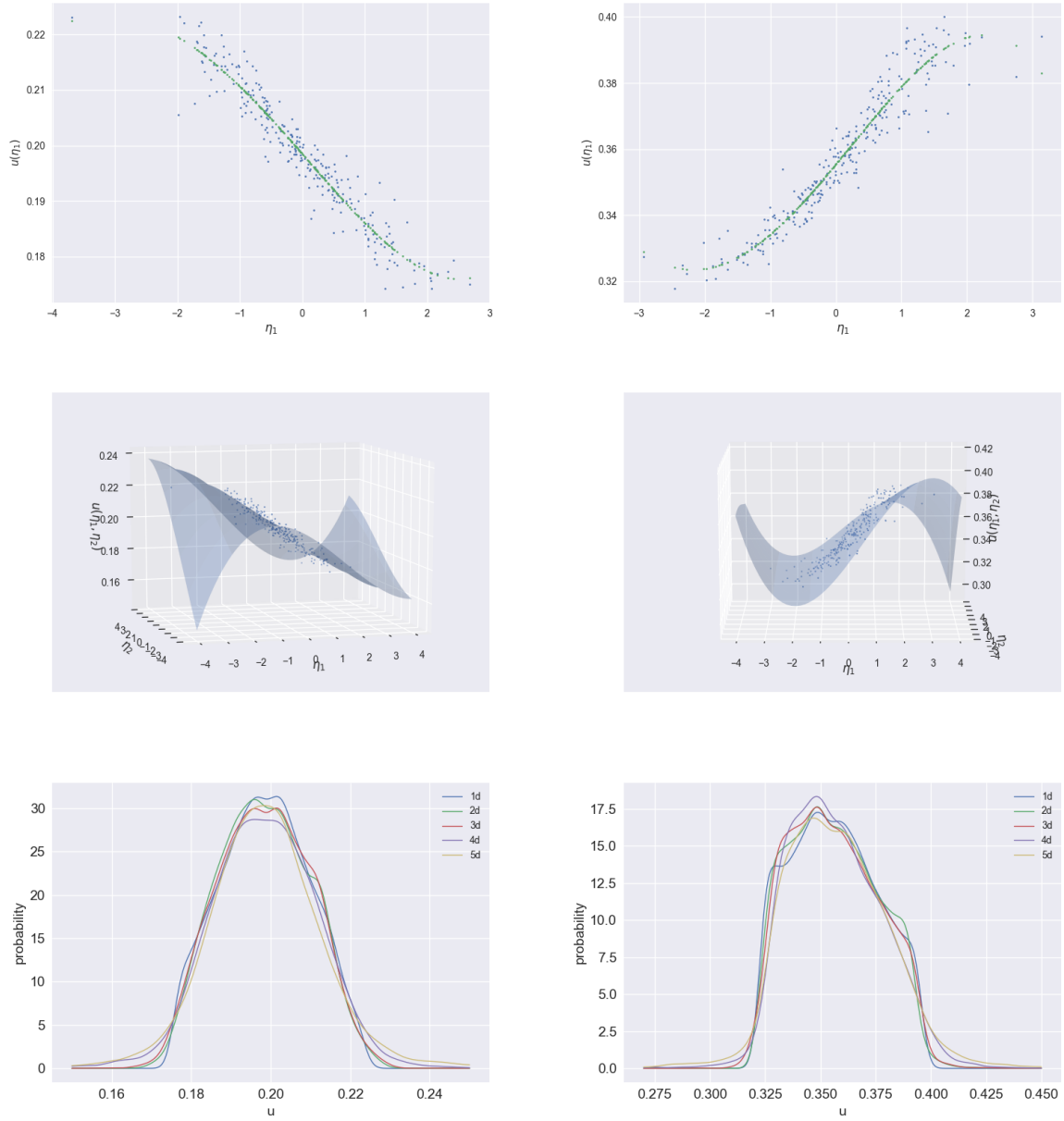


Figure 10: Top: 1D chaos expansions with rotated inputs evaluated at the input data points. Middle: 2D chaos expansions with rotated inputs evaluated over the $[-4, 4]^2$ domain. The datapoints in both cases are plotted as functions of the rotated inputs. Bottom: Density functions for up to 5D chaos expansions. Left column results corresponds to ϕ_B while right column corresponds to R_P .

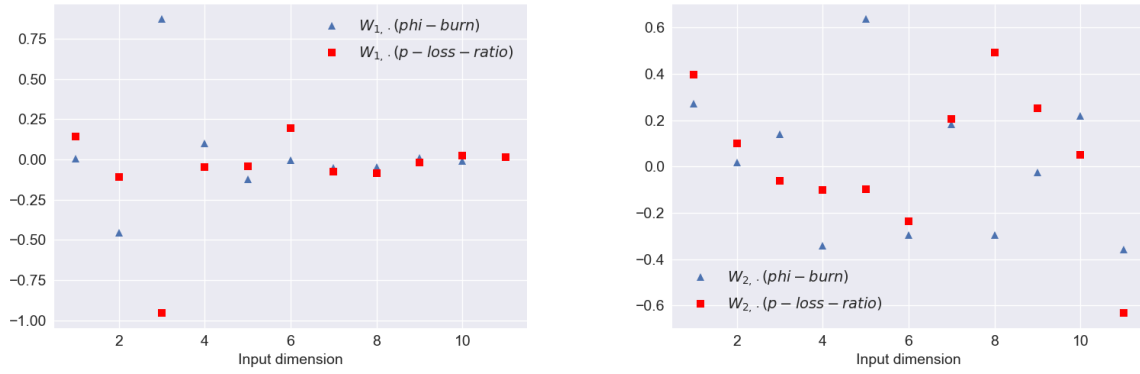


Figure 11: Comparison of the values of the first (left) and second (right) rows of the projection matrix for the two QoIs.

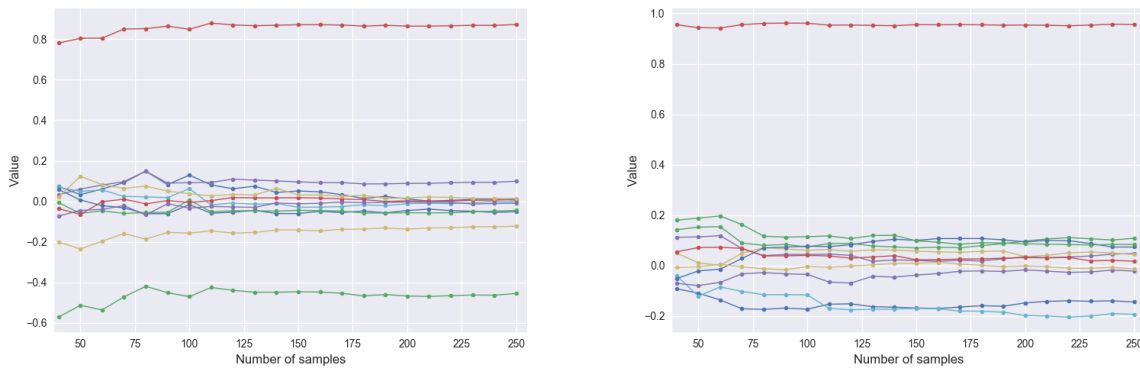


Figure 12: Estimated projection vector values of the 1D expansion versus number of samples used for ϕ_B (left) and $R_{\bar{P}}$ (right).

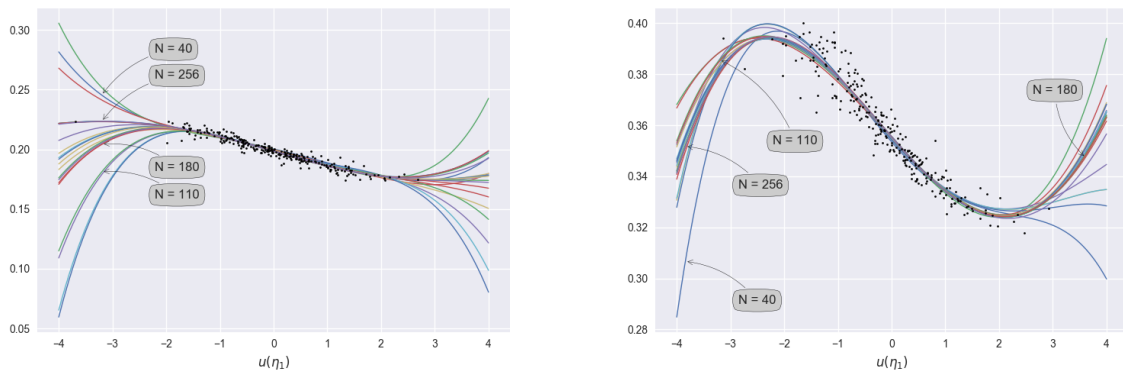


Figure 13: Plots of all the 1D PC expansions of ϕ_B (left) and $R_{\bar{P}}$ (right), computed for a number of samples varying from $N = 40$ to $N = 256$. All 256 samples are also shown.

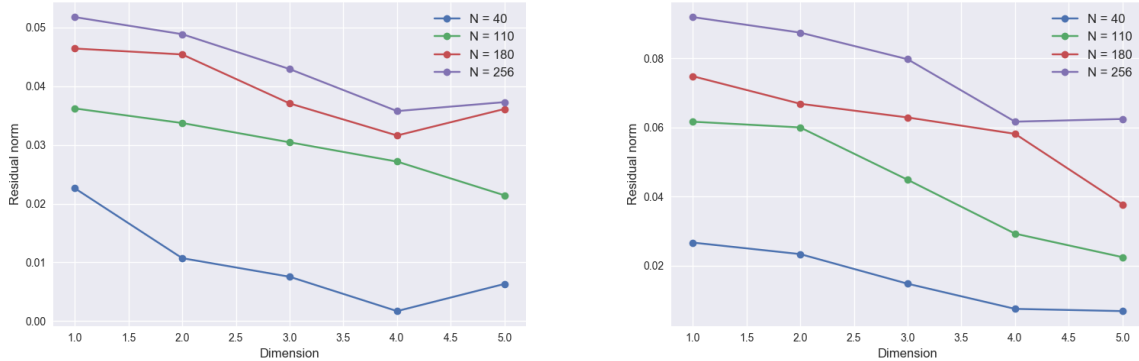


Figure 14: Plots of ℓ_2 residuals versus dimensionality with $N = 40, 110, 180$ and 256 for ϕ_B (left) and $R_{\bar{P}}$ (right).

Appendix B. On the equivalence of solutions of the ℓ_2 error

Here we explain in some more detail the connection between Algorithms 2 and 3. Assume that \mathbf{c}^* and \mathbf{W}^* are the outcome of Alg. 2. For the corresponding expansion

$$u(\tilde{\boldsymbol{\eta}}) = \sum_{\boldsymbol{\alpha}} c_{\boldsymbol{\alpha}} \psi_{\boldsymbol{\alpha}}(\tilde{\boldsymbol{\eta}}) \quad (\text{B.1})$$

with $\tilde{\boldsymbol{\eta}} = \mathbf{W}^* \boldsymbol{\xi}$, let \mathbf{B} be any $d_0 \times d_0$ isometry matrix and set $\boldsymbol{\zeta} = \mathbf{B} \tilde{\boldsymbol{\eta}}$. The expansion can be rewritten as

$$u(\boldsymbol{\eta}) \stackrel{a.s.}{=} \hat{u}(\boldsymbol{\zeta}) = \sum_{\boldsymbol{\beta}} \hat{c}_{\boldsymbol{\beta}} \psi_{\boldsymbol{\beta}}(\boldsymbol{\zeta}). \quad (\text{B.2})$$

Denoting with $\hat{\mathbf{c}}$ the vector of new coefficients and with $\Psi_{\mathbf{B}\mathbf{W}^*}$ the new measurement matrix and using the almost sure equality of the two expansions we get that

$$\min_{\mathbf{W}} \|\mathbf{u} - \Psi_{\mathbf{W}} \mathbf{c}\|_2 = \|\mathbf{u} - \Psi_{\mathbf{W}^*} \mathbf{c}^*\|_2 = \|\mathbf{u} - \Psi_{\mathbf{B}\mathbf{W}^*} \hat{\mathbf{c}}\|_2 \quad (\text{B.3})$$

that is $\mathbf{B}\mathbf{W}^*$ provides the same fit on the data. Intuitively, Alg. 2 can attain a particular minimum for many different rotation matrices, depending each time on the starting values of \mathbf{W} which in general are chosen randomly. Equality of the corresponding coefficients of course is not guaranteed. Each set of coefficients attains a minimum ℓ_1 norm only for the corresponding $\Psi_{\mathbf{W}}$.

References

- [1] Doostan A., Ghanem R., and J. Red-Horse. Stochastic model reduction for chaos representations. *Computer Methods in Applied Mechanics and Engineering*, 196(37-40):3951–3966, 2007.
- [2] M. Arnst, R. Ghanem, E. Phipps, , and J. Red-Horse. Measure transformation and efficient quadrature in reduced-dimensional stochastic modeling of coupled problems. *International Journal for Numerical Methods in Engineering*, 92(12):1044–1080, 2012.
- [3] I. Babuška, F. Nobile, and R. Tempone. A stochastic collocation method for elliptic partial differential equations with random input data. *SIAM Journal on Numerical Analysis*, 45:1005–1034, 2007.
- [4] G. Blatman and B. Sudret. Adaptive sparse polynomial chaos expansion based on least angle regression. *Journal of Computational Physics*, 230:2345–2367, 2011.
- [5] R. Cameron and W. Martin. The orthogonal development of nonlinear functionals in series of fourier-hermite functionals. *Annals of Mathematics*, 48:385–392, 1947.
- [6] Emmanuel J. Candès, Justin Romberg, and Terence Tao. Robust Uncertainty Principles: Exact Signal Reconstruction From Highly Incomplete Frequency Information. *IEEE Transactions on Information Theory*, 52(2):489–509, 2006.

- [7] K. Chowdhary and H.N. Najm. Bayesian estimation of karhunenlove expansions; a random subspace approach. *Journal of Computational Physics*, 319:280–293, 2016.
- [8] P.L. Combettes and J.C. Pesquet. A Douglas - Rachford splitting approach to nonsmooth convex variational signal recovery. *IEEE Journal of Selected Topics in Signal Processing*, 1:564–574, 2007.
- [9] P. G. Constantine, E. Dow, and Q. Wang. Active subspace methods in theory and practice: applications to kriging surfaces. *SIAM Journal on Scientific Computing*, 36:A1500–A1524, 2014.
- [10] P.G. Constantine, M. Emory, J. Larsson, and G. Iaccarino. Exploiting active subspaces to quantify uncertainty in the numerical simulation of the hyshot ii scramjet. *Journal of Computational Physics*, 302:1–20, 2015.
- [11] Douglas J. Dolvin. Hypersonic International Flight Research and Experimentation (HIFiRE). In *15th AIAA International Space Planes and Hypersonic Systems and Technologies Conference*, number 2008-2581, Dayton, OH, 2008.
- [12] Douglas J. Dolvin. Hypersonic International Flight Research and Experimentation. In *16th AIAA/DLR/DGLR International Space Planes and Hypersonic Systems and Technologies Conference*, number 2009-7228, Bremen, Germany, 2009.
- [13] D.L. Donoho. Compressed sensing. *IEEE Transactions on information theory*, 52:1289–1306, 2006.
- [14] D.L. Donoho, M. Elad, and V.N. Temlyakov. Stable recovery of sparse overcomplete representations in the presence of noise. *IEEE Transactions on information theory*, 52:6–18, 2006.
- [15] A. Doostan and G. Iaccarino. A least-squares approximation of partial differential equations with high-dimensional random inputs. *Journal of Computational Physics*, 228:4332–4345, 2009.
- [16] A. Doostan and H. Owhadi. A non-adapted sparse approximation of pdes with stochastic inputs. *Journal of Computational Physics*, 230:3015–3034, 2011.
- [17] J. Douglas and H.H. Rachford. On the numerical solution of heat conduction problems in two and three space variables. *Transactions of the American mathematical Society*, 82:421–439, 1956.
- [18] R. Ghanem. Scales of fluctuation and the propagation of uncertainty in random porous media. *Water Resources Research*, 34:2123–2136, 1998.
- [19] R. Ghanem. Ingredients for a general purpose stochastic finite elements implementation. *Computer Methods in Applied Mechanics and Engineering*, 168:19–34, 1999.
- [20] R. Ghanem and S. Dham. Stochastic finite element analysis for multiphase flow in heterogeneous porous media. *Transport in Porous Media*, 32:239–262, 1998.
- [21] R. Ghanem and J. Red-Horse. Propagation of probabilistic uncertainty in complex physical systems using a stochastic finite element approach. *Physica D: Nonlinear Phenomena*, 133:137–144, 1999.
- [22] R. Ghanem and P. Spanos. *Stochastic finite elements: A spectral approach*. Springer-Verlag, 1991.
- [23] D. Ghosh and R. Ghanem. Stochastic convergence acceleration through basis enrichment of polynomial chaos expansions. *International Journal of Numerical methods in Engineering*, 73(2):162–184, 2008.
- [24] Mark R. Gruber, Kevin Jackson, and Jiwen Liu. Hydrocarbon-Fueled Scramjet Combustor Flowpath Development for Mach 6-8 HIFiRE Flight Experiments. Technical report, AFRL, 2008.
- [25] N. Hass, K. Cabell, A. Storch, and M. Gruber. Hifire direct-connect rig (hdcr) phase i scramjet test results from the nasa langley arc-heated scramjet test facility. In *In 17th AIAA international space planes and hypersonic systems and technologies conference (p. 2248)*, 2011.
- [26] X. Huan, C. Safta, K. Sargsyan, G. Geraci, M.S. Eldred, Z.P. Vane, G. Lacaze, J.C. Oefelein, and H.N. Najm. Global sensitivity analysis and quantification of model error in scramjet computations. arXiv preprint arXiv:1707.09478, 2017.
- [27] X. Huan, C. Safta, K. Sargsyan, Z.P. Vane, G. Lacaze, J.C. Oefelein, and H.N. Najm. Compressive sensing with cross-validation and stop-sampling for sparse polynomial chaos expansions. arXiv preprint arXiv:1707.09334, 2017.
- [28] J.D. Jakeman, M.S. Eldred, and K. Sargsyan. Enhancing ℓ_1 -minimization estimates of polynomial chaos expansions using basis selection. *Journal of Computational Physics*, 289:18–34, 2015.
- [29] Guilhem Lacaze, Zachary P. Vane, and Joseph C. Oefelein. Large Eddy Simulation of the HIFiRE Direct Connect Rig Scramjet Combustor. In *55th AIAA Aerospace Sciences Meeting*, number 2017-0142, Grapevine, TX, 2017.
- [30] O.P. Le Maître, M.T. Reagan, H.N. Najm, R.G. Ghanem, and O.M. Knio. A stochastic projection method for fluid flow: Ii. random process. *Journal of Computational Physics*, 181:9–44, 2002.
- [31] Y. M. Marzouk, H. N. Najm, and L. Rahn. Stochastic spectral methods for efficient bayesian solution of inverse problems. *Journal of Computational Physics*, 224:560–586, 2007.
- [32] H.N. Najm. Uncertainty quantification and polynomial chaos techniques in computational fluid dynamics. *Annual Review of Fluid Mechanics*, 41:35–52, 2009.
- [33] J. Nocedal and S. Wright. *Numerical optimization*. Springer Science & Business Media, 2006.
- [34] J.C. Oefelein. *Simulation and analysis of turbulent multiphase combustion processes at high pressures*. PhD thesis, Pennsylvania State University, University Park, Pennsylvania, May 1997.
- [35] J.C. Oefelein. Large eddy simulation of turbulent combustion processes in propulsion and power systems. *Progress in Aerospace Sciences*, 42:2–37, 2006.
- [36] K. Pearson. Liii. on lines and planes of closest fit to systems of points in space. *The London, Edinburgh, and Dublin Philosophical Magazine and Journal of Science*, 2:559–572, 1901.
- [37] Gerald L. Pellett, Sarah N. Vaden, and Lloyd G. Wilson. Opposed Jet Burner Extinction Limits: Simple Mixed Hydrocarbon Scramjet Fuels vs Air. In *43rd AIAA/ASME/SAE/ASEE Joint Propulsion Conference & Exhibit*, number 2007-5664, Cincinnati, OH, 2007.
- [38] J. Peng, J. Hampton, and A. Doostan. A weighted 1-minimization approach for sparse polynomial chaos expansions. *Journal of Computational Physics*, 267:92–111, 2014.
- [39] C.E. Rasmussen and C.K. Williams. *Gaussian processes for machine learning (Vol. 1)*. Cambridge: MIT press, 2006.

- [40] M.T. Reagan, H.N. Najm, R.G. Ghanem, and O.M. Knio. Uncertainty quantification in reacting-flow simulations through non-intrusive spectral projection. *Combustion and Flame*, 132:545–555, 2003.
- [41] A. Saltelli, M. Ratto, T. Andres, F. Campolongo, J. Cariboni, D. Gatelli, M. Saisana, and S. Tarantola. *Global sensitivity analysis: the primer*. John Wiley & Sons, 2008.
- [42] K. Sargsyan, C. Safta, H.N. Najm, B.J. Debusschere, D. Ricciuto, and P. Thornton. Dimensionality reduction for complex models via bayesian compressive sensing. *International Journal for Uncertainty Quantification*, 4, 2014.
- [43] P.R. Spalart, W.H. Jou, M. Strelets, and S.R. Allmaras. Comments on the feasibility of LES for wings, and on a hybrid RANS/LES approach. *Advances in DNS/LES*, 1:4–8, 1997.
- [44] Andrea M. Storch, Michael Bynum, Jiwen Liu, and Mark Gruber. Combustor Operability and Performance Verification for HIFiRE Flight 2. In *17th AIAA International Space Planes and Hypersonic Systems and Technologies Conference*, number 2011-2249, San Francisco, CA, 2011.
- [45] C. Thimmisetty, P. Tsilifis, and R. Ghanem. Homogeneous chaos basis adaptation for design optimization under uncertainty: Application to the oil well placement problem. *AI EDAM*, 31:265–276, 2017.
- [46] R. Tibshirani. Regression shrinkage and selection via the lasso. *Journal of the Royal Statistical Society. Series B (Methodological)*, pages 267–288, 1996.
- [47] R. Tipireddy and R.G. Ghanem. Basis adaptation in homogeneous chaos spaces. *Journal of Computational Physics*, 259:304–317, 2014.
- [48] R. Tripathy, I. Bilionis, and M. Gonzalez. Gaussian processes with built-in dimensionality reduction: Applications to high-dimensional uncertainty propagation. *Journal of Computational Physics*, 321:191–223, 2016.
- [49] P. Tsilifis and R.G. Ghanem. Reduced wiener chaos representation of random fields via basis adaptation and projection. *Journal of Computational Physics*, 341:102–120, 2017.
- [50] Zaiwen Wen and Wotao Yin. A feasible method for optimization with orthogonality constraints. *Mathematical Programming*, 142:397–434, 2013.
- [51] N. Wiener. The homogeneous chaos. *American Journal of Mathematics*, 60:897–936, 1938.
- [52] Jeroen Witteveen, Karthik Duraisamy, and Gianluca Iaccarino. Uncertainty Quantification and Error Estimation in Scramjet Simulation. In *17th AIAA International Space Planes and Hypersonic Systems and Technologies Conference*, number 2011-2283, 2011.
- [53] D. Xiu and G.E. Karniadakis. Modeling uncertainty in flow simulations via generalized polynomial chaos. *Journal of Computational Physics*, 187:137–167, 2003.
- [54] R.J. Yentsch and D.V. Gaitonde. Exploratory simulations of the hifire 2 scramjet flowpath. In *48th AIAA/ASME/SAE/ASEE Joint Propulsion Conference and Exhibit*, July 2012.